# Use of enhanced-resolution QuikScat/SeaWinds data for operational ice services and climate research: sea ice edge, type, concentration and drift.

Jörg Haarpaintner
Norut IT
Tromsø, Norway
Joerg.Haarpaintner@itek.norut.no

Marcos Porcires
Met.no
Tromsø, Norway
marcosp@met.no

*Abstract*— **Enhanced resolution QuikScat/SeaWinds (QS$_{er}$) data recently entered the daily ice chart operation of the national ice services. Algorithms have been developed to extract four important sea ice parameters from this data over the whole Arctic: sea ice edge, type, concentration and drift. This paper will summarize the different algorithms with a more detailed presentation of the sea ice concentration algorithm. The sea ice edge can be detected to ice concentration as low as 10%. Sea ice types can be roughly separated by a single threshold of –13 dB in the horizontal polarization. The ice concentration algorithm gives reasonable qualitative results, separating well into high and low ice concentrations in general and resolves even some characteristic ice features in the Marginal Ice Zone (MIZ) and dynamic areas like the Fram Strait. Sea ice drift can be determined with an accuracy of about 2.6 cm/s for a 48h drift.**

*Keywords- sea ice, Arctic, scatterometry, remote sensing.*

## I. INTRODUCTION

Sea ice plays a key role in the earth's climate and its observation by satellite remote sensing techniques is an important task in climate research. Additionally, sea ice presents a major risk for marine activities and the national ice services are required to produce reliable ice charts to secure navigation and other offshore activities. Especially microwave sensors are crucial tools because of their independence of sunlight and cloud-penetrating capability. The SeaWinds instrument on QuikScat (QS) is an active Ku-band dual-polarized, scanning pencil-beam scatterometer, operating at 13.4 GHz in horizontal (HH) and vertical (VV) polarization, with swath widths of 1400 km and 1800 km, respectively. The 25 km x 37 km footprint can be divided by range Doppler filtering into 25 km x 6 km slices. Additional filtering, sub-sampling and averaging over a 36h period produces average and standard deviation images on a 2.225-km grid for both polarizations covering the Arctic and Antarctic on a daily basis [1][2]. These enhanced resolution products (QS$_{er}$) are distributed in near-real time by the National Environmental Satellite Data and Information System (NESDIS). Based on these four daily image products as well as on the derived active polarization ratio (APR), algorithms to detect four among the most important sea ice parameters, sea ice edge, type, concentration, and drift, have been developed for the Arctic.

These algorithms are run operationally at the ice service of the Norwegian Meteorological Institute. Together with ice concentrations derived from the Advanced Microwave Scanning Radiometer for EOS (AMSR-E) on Aqua and high-resolution synthetic aperture radar imagery from Envisat and Radarsat, these QS$_{er}$ sea ice products are today a crucial data set for reliable sea ice monitoring.

In this paper we will summarize these algorithms and their results. The sea ice concentration algorithm [3] will be presented more explicitly since the sea ice edge and drift algorithm have already been published in detail in earlier publications [4][5].

## II. SEA ICE EDGE

A first version for ice-ocean discrimination from QS$_{er}$ has been developed in [6], but it detected neither low ice concentration, nor thin ice [7]. A refined version to detect also low ice concentrations has been developed [4].

All measurement variables, i.e. the backscatter in HH and VV polarizations, their polarization ratio and the daily standard deviation of the HH and VV backscatters are sensitive to ice types and strongly correlated with the ice concentration [8]. The active polarization ratio (APR) has been defined in [9] as APR = $(\sigma_{0H} - \sigma_{0V}) / (\sigma_{0H} + \sigma_{0V})$, where $\sigma_{0H}$ and $\sigma_{0V}$ are the backscatter values expressed as power in linear scale. APR showed to be the crucial variable to separate ice from ocean with a threshold of –0.02. Season-dependant thresholds for the other variables serve to eliminate most of the ocean noise, i.e. ocean pixels falsely classified as ice. The effective QS$_{er}$ resolution is estimated to 5-10 km but the QS$_{er}$ products are sub-sampled on a 2.225 km grid. Reducing the ice edge resolution to a 6.675 km grid by averaging over a 3x3 pixel window allows us to choose the least ambiguous that is the highest absolute APR value among the 3x3 pixels. The history of the ice cover is also used to detect individual ice fields that are separated from the Arctic pack and would otherwise be eliminated by filtering. Fig. 1a shows an example of the sea ice edge detection over the whole Arctic from 11 March 2003 The validation study showed that ice concentrations as low as 10% can be detected by this algorithm. Strong melting events during summer can cause strong daily variations in the backscatter and increase the daily standard deviation and thus falsely classify

ice as open water. However, such errors can be easily eliminated by comparing subsequent days.

## III. Sea Ice Type

Multi-year (MYI) and first-year (FYI) ice have different salt contents. Since scatterometer radar pulses have a deeper penetration depth in fresh ice than in ice containing brine pockets, the backscatter of MYI is characterized by stronger volume scattering than FYI and appears therefore brighter in the satellite images. A good threshold for separating MYI from FYI is about −13 dB [4]. Other factors, like flushing, melting and refreezing of the surface ice layer can, however, also change the salt water content in the ice and can be independent of the ice age. In the Arctic, such events occur mainly in the marginal ice zone or during summer. Fig. 1b shows the classified image of Fig. 1a into FYI and MYI.
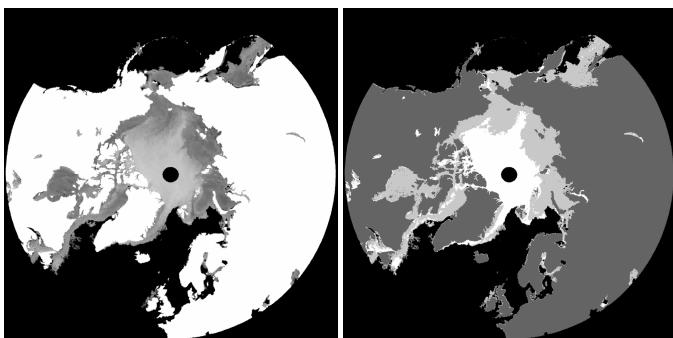


Figure 1. Arctic sea ice cover from 11 March 2003: a) $\sigma_{0H}$ and b) classified into FYI (light grey) and MYI (white).

## IV. Sea Ice Concentration

$QS_{er}$ products were co-located and statistically analyzed with Special Sensor Microwave/Imager (SSM/I) NASA-Team ice concentration maps over the whole Arctic ice cover. The statistical analysis revealed that there is an obvious signature of the total ice concentration in the available QS parameters: $\sigma_{0H}$, $\sigma_{0V}$, $STD_{HH}$, $STD_{VV}$ and APR (Fig. 2). Exponential regression lines (in red) between the monthly averaged QS variables and SSM/I ice concentration revealed correlation coefficients $R^2$ greater than 0.95 (Fig. 2). The regression equations are used to determine the ice concentration from QS data alone for the whole Arctic at 6.675-km resolution (1) for each individual parameter and (2) for a combination of different parameters and their regression equations.

### A. Ice concentration (IC) from individual QS parameters

The ice concentration from the individual parameters $\sigma_{0H}$, mean($STD_{HH}$, $STD_{VV}$), and APR are described here.

#### 1) $IC_{HH}$

Fig. 2a shows that the backscatter increases with higher ice concentrations. As said earlier the backscatter is mainly driven by the ice type. When averaged over the whole Arctic, there is also a correlation between the ice type composition and the total ice concentration. More MYI is generally present in higher ice concentrations. Studying the derived ice concentration from $\sigma_{0H}$ alone shows therefore that it

corresponds more to the MYI fraction than to the real ice concentration. In addition, surface roughness has also a strong impact on the backscatter and ridged FYI fields appear therefore also as higher ice concentration. $\sigma_{0H}$ is therefore unsuitable to determine ice concentration by itself. The same is also the case for $\sigma_{0V}$.
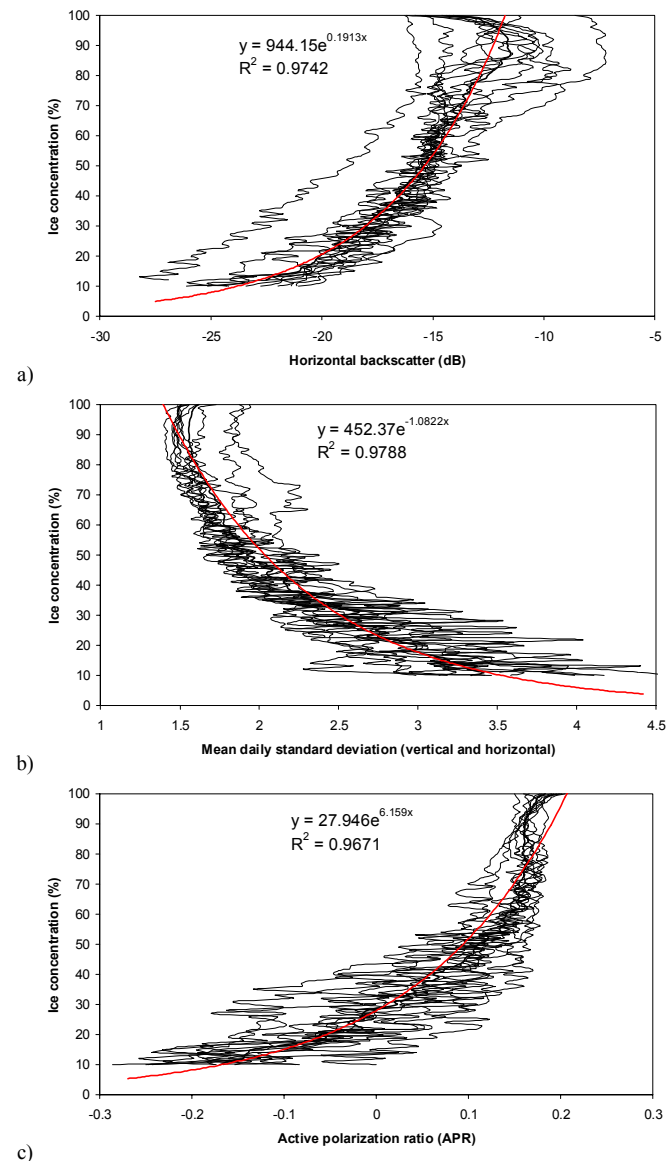


Figure 2. Co-location of NT ice concentration and QS variables: (a) $\sigma_{0H}$, (b) $\sigma_{0V}$, (c) STD and (d) APR. The thin lines are daily mean values for each ice concentration for the first day of all months. The thick lines are the average of the thin lines and the red line is the regression line with indicated equation.

#### 2) $IC_{STD}$

$STD_{HH}$ and $STD_{VV}$ are similar and we use therefore their mean value (STD) in this comparison. Fig. 2b shows that STD decreases with higher ice concentrations. STD is mainly dominated by the daily backscatter variation over open water due to the highly variable ocean surface as well as the different azimuth angles of the multiple observations per pixel. Inside the pack ice, STD is slightly lower for MYI than for FYI because of stronger surface scattering for FYI. Its derived ice
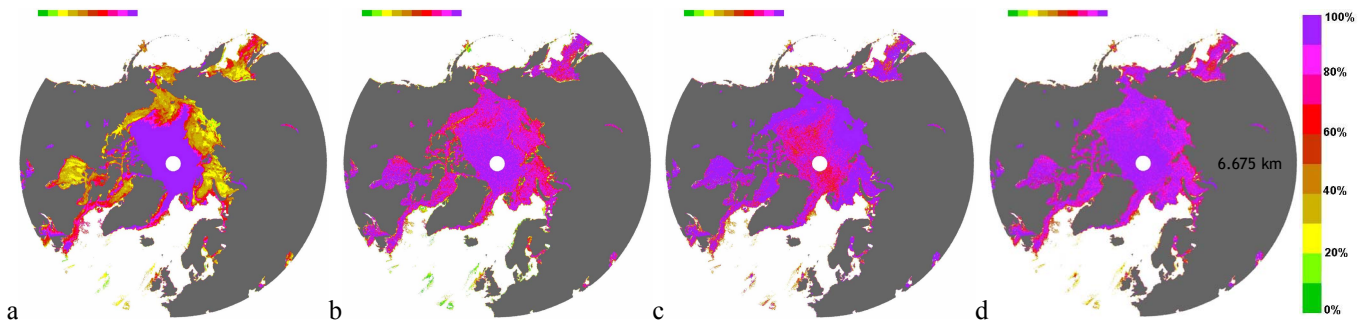
Figure 3. Ice concentration maps from individual parameters (a) $IC_{HH}$, (b) $IC_{STD}$, (c) $IC_{APR}$ and (d) from the combination of all of them on 11 March 2003.
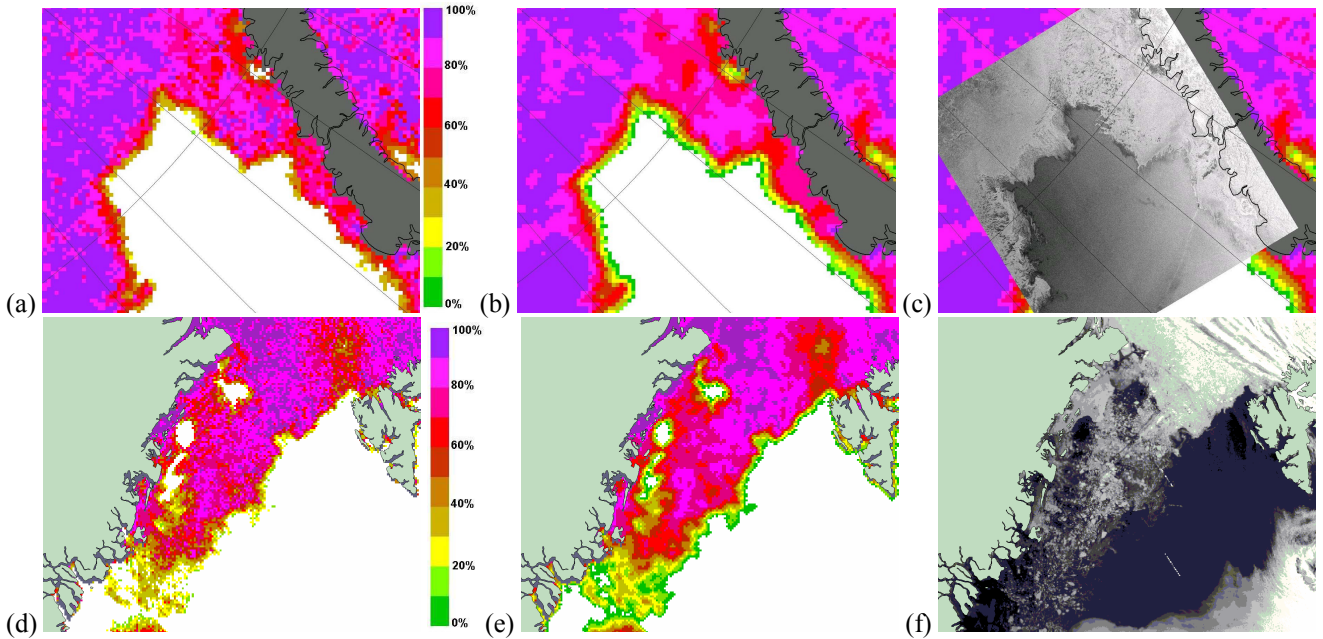


Figure 4. Ice concentration results in (a) 6.675-km and (b) 20-km resolution compared to a (c) Radarsat SAR image (©CSA) in the eastern Barents Sea in winter (11 March 2003) and (d) 6.675-km (e) 20-km resolution compared to a (f) AVHRR (©NOAA) image (1 km res.) in Fram Strait in summer (21 July 2003).

concentration is therefore slightly higher. Along the MYI/FYI border, STD increases due to dynamics in the ice cover, the strong variation along the MYI/FYI border, and shows therefore lower ice concentration. Along the MIZ, the effect of higher STD over open water seems to give reasonable results in order to reflect the ice concentration.

*3) $IC_{APR}$*

Fig. 2c shows higher APR values with higher ice concentrations. APR is higher for FYI than for MYI [4]. FYI regions appear therefore as higher ice concentration and APR varies little for ice concentration above 50%. Below 50% however, it seems that the open ocean has a stronger effect, i.e. reducing the APR, than the different ice types. The APR seems therefore to be a reliable parameter to determine ice concentration in the MIZ.

*B.  Combining the different parameters to determine the ice concentration.*

It was shown that the individual parameters were unreliable alone to determine the ice concentration over the whole Arctic region. However, each of them presented some characteristics

for different ice regions that could be used in a combination of all of them to determine the ice concentration from QS. We divide the Arctic ice cover first in these regions that are regions of different ice types, MYI and FYI, and the MIZ. The FY/MYI areas are separated by $\sigma_{0H}(FYI) < -13dB < \sigma_{0H}(MYI)$. We define the MIZ as a 20-pixel (~125 km) large belt along the ice edge. We then propose the following empirical combinations of the ice concentrations (IC) from the individual parameters, based on the results above.

$$IC(MYI) = max(IC_{APR}, IC_{STD})$$

$$IC(FYI) = (max(IC_{HH}, IC_{STD}) + IC_{APR}) / 2$$

$$IC(MIZ) = (IC_{HH} + IC_{STD} + IC_{APR}) / 3,$$

Where $IC_{HH}$, $IC_{STD}$, $IC_{APR}$ are the ice concentrations from the individual parameters alone. Fig. 3 shows the Arctic ice concentration for each individual parameter and for the combination for 11 March 2003.

*C.  Results*

To adapt the ice concentration to the usual 20 km ice concentration from SSM/I, Fig. 4 shows the ice concentration

results in 6.675 km and 20 km resolution compared to higher resolution satellite imagery. Although very empirical, the combined ice concentration gives qualitatively reasonable results, separating well into high and low ice concentrations: high ice concentration (> 80%) over the whole Arctic pack ice and decreasing ice concentration in the MIZ towards the ice edge. Some individual ice features could even be resolved in the highly dynamic Fram Strait during summer, including polynyas and very low ice concentration in the Greenland Sea. Quantitatively however the ice concentrations are presumably not very accurate since high variations occur in the pack ice. A full validation however still needs to be done.

## V. SEA ICE DRIFT

Sea ice drift can be determined from $QS_{er}$ imagery by maximum cross-correlation (MCC) [5]. Correlation windows of 61x61 pixel have been used to calculate the MCC for both polarizations independently for images separated by 2 days. Erroneous drift vectors can easily be eliminated by comparing the two resulting 48h ice drift vectors, $\overrightarrow{u_{VV}}$ and $\overrightarrow{u_{HH}}$. Additional filtering is performed by setting a minimum correlation coefficient and by considering the spatial consistency of the motion field. Eliminated vectors will be reconstructed by interpolation. The results have been validated by IABP buoys showing an error standard deviation in ice drift speed of 2.6 cm/s for a 48h drift. Errors are largest in dynamic regions with low ice concentrations like the southern Fram Strait. Fig. 5 shows an example of ice drift in the European Arctic with the transpolar drift and the Fram Strait outflow. Ice drift data derived from $QS_{er}$ have been used in connection with ice thickness measurements from ICESat in order to estimate the sea ice volume flux through Fram Strait in 2003 [10] with results comparable to historical mean values [11].
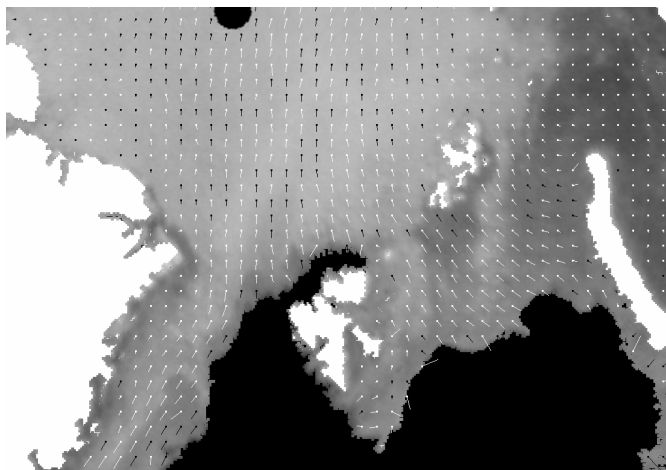


Figure 5. 48h $QS_{er}$ ice drift in the European Arctic from 11-13 March 2003. White drift vectors (flags) are calculated by MCC, black drift vectors are filtered and then interpolated drift vectors.

## VI. CONCLUSION

In this paper we summarized the algorithms to extract four important sea ice parameters (edge, type, concentration and drift) from $QS_{er}$ data with a more detailed description of the sea ice concentration algorithm. Ice thickness cannot be determined from QS. These algorithms have been implemented in the daily operations at the Met.no ice service and significantly improved the accuracy of the produced sea ice charts. QS has been operational since 1999 and presents therefore also an important data set for climate research. Unfortunately ADEOS-II who carried the follow-up of the SeaWinds sensor failed nine months after its launch in 2003 and the continuity of this data set is at risk. The upcoming European series of polar orbiting satellites for operational meteorology (MetOp) will carry the Advanced SCATterometer (ASCAT) and will hopefully provide a continuous scatterometer data set from the first launch in 2006 until 2019. A future challenge is to adapt these algorithms to ASCAT who operates in C-band single polarization. It is planned that enhanced resolution products will also be produced from ASCAT.

## REFERENCES

[1] D.G. Long, P.J. Hardin, and P.T. Whiting, "Resolution enhancement of spaceborne scatterometer data," IEEE Trans. Geosci. Remote Sens., vol. 31, no. 3, pp. 700-715, 1993.

[2] D.S. Early, and D.G. Long, "Image reconstruction and enhanced resolution imaging from irregular samples," IEEE Trans. Geosci. Remote Sensing, vol. 39(2), pp. 291-302, 2001.

[3] J. Haarpaintner, and M. Porcires, "On the Sea Ice Concentration from enhanced resolution QuikScat/Seawinds data," Oral presentation at the European Geosciences, 1st General Assembly Union , Nice, France, 25-30 April 2004.

[4] J. Haarpaintner, R.T. Tonboe, D.G. Long, and M.L. VanWoert, "Automatic detection and validity of the sea ice edge: an application of enhanced resolution QuikScat/SeaWinds data," IEEE Trans. Geosci. Remote Sensing, vol. 42(7), 1433-1443, 2004.

[5] J. Haarpaintner, "Arctic-Wide Operational Sea Ice Drift from Enhanced Resolution QuikScat/SeaWinds Scatterometry and its Validation," IEEE Trans. Geosci. Remote Sensing, vol. 44(1), 102-107, 2006.

[6] Q.P. Remund, and D.G. Long, "Sea ice extent mapping using Ku-band scatterometer data," J. Geophys. Res., vol. 104(C5), pp. 11,515-11,527, 1999.

[7] R. De Abreu, K. Wilson, M. Arkett, and D. Langlois, "Evaluating the use of QuikSCAT data for operational sea ice monitoring," in Proceedings of the 2002 IEEE International Geoscience and Remote Sensing Symposium, Toronto, Canada, June 2002.

[8] R. Tonboe and J. Haarpaintner, "Implementation of QuikScat/SeaWinds data in the EUMETSAT Ocean & Sea Ice ice product," Danish Meteorological Institute, Copenhagen, Denmark, Technical Report, No. 03-13, 41 pp., 2003.

[9] R. Tonboe and R. Ezraty, "Monitoring of new-ice in Greenland waters," in Proceeding of the 2002 IEEE International Geoscience and Remote Sensing Symposium, Toronto, Canada, June 2002, pp 1932-1934, 2002.

[10] G. Spreen, S. Kern, D. Stammer, R. Forsberg, and J. Haarpaintner, "Satellite-based estimates of sea ice volume flux through Fram Strait," Ann. Glaciol., 44, in press, 2006.

[11] R. Kwok, G.F. Cunningham, and S.S. Pang, "Fram Strait sea ice outflow," J. Geophy. Res., vol. 109, no. C01009, 2004.